

A Highly Selective And Sensitive Pyrazole-Based Chemosensor For Naked-Eye And Spectroscopic Detection Of CU (II) Ions

Ranjith Kore¹, D. Venkateshwar Rao¹ And Someshwar Pola^{1*}

Department Of Chemistry, University College Of Science, Osmania University, Hyderabad, 500007, Telangana, India.

Abstract:

A novel pyrazole derivative, 3-(1,3-bis(4-bromophenyl)-1H-pyrazol-4-yl)-2-(4-bromophenyl) acrylonitrile (BPPBPA), has been successfully synthesized and investigated as a highly selective and sensitive chemosensor for the detection of Cu (II) ions. Both absorption and emission spectroscopic studies clearly demonstrate the sensing capabilities of BPPBPA. Upon interaction with Cu (II) ions, the absorption spectrum exhibited a noticeable red-shift in wavelength accompanied by a decrease in intensity, indicating complex formation. Concurrently, the emission spectrum showed significant quenching, attributed to the coordination of Cu (II) ions with the pyrazole ring nitrogen atoms and the inherent paramagnetic nature of Cu (II). Further experimental evidence from Vibrating Sample Magnetometry (VSM) studies corroborated the paramagnetic characteristics of the BPPBPA-Cu (II) complex. The successful formation of the BPPBPA-Cu (II) complex was definitively confirmed through X-ray Photoelectron Spectroscopy (XPS), ESR and VSM analysis. This work highlights BPPBPA as a promising candidate for the selective and sensitive optical detection of Cu (II) ions in various applications.

Key Word: BPPBPA Molecule; X-ray Photoelectron Spectroscopy (XPS); ESR; Vibrating Sample Magnetometry VSM; chemosensor; Cu (II) ion Detection.

Date of Submission: 28-05-2025

Date of Acceptance: 08-06-2025

I. Introduction

The accurate and rapid detection of heavy metal ions in environmental, biological, and industrial matrices have become a paramount concern in modern analytical chemistry [1]. Among these, copper (Cu (II)) ions pose a unique challenge due to their dual nature; while essential for numerous biological processes at trace levels, elevated concentrations can lead to severe environmental pollution and detrimental health effects, including oxidative stress, neurodegenerative diseases, and organ damage [2]. The widespread use of copper in industries such as electroplating, mining, agriculture, and electronics inevitably leads to its release into water bodies, necessitating robust and reliable monitoring strategies [3]. Consequently, the development of highly selective, sensitive, and cost-effective methods for Cu (II) detection is of immense importance, driving intense research efforts across various scientific disciplines.

Traditional methods for heavy metal detection, such as atomic absorption spectrometry (AAS), inductively coupled plasma-mass spectrometry (ICP-MS), and X-ray fluorescence (XRF), offer high sensitivity and accuracy [4-14]. However, these techniques often suffer from drawbacks such as high instrumentation costs, complex sample preparation procedures, the need for specialized personnel, and limited portability, making them less suitable for on-site or real-time monitoring applications. In light of these limitations, the burgeoning field of chemosensor development has emerged as a promising alternative, offering the potential for simple, rapid, and visually detectable responses to target analytes. Chemosensors, particularly those operating via optical mechanisms, leverage the selective interaction between a recognition probe and an analyte to produce a measurable change in an optical signal, such as absorption, fluorescence, or color [15]. This approach enables convenient and often naked-eye detection, making them highly desirable for diverse applications, from environmental monitoring to clinical diagnostics [16-17].

The design of effective chemosensors hinges critically on the rational selection and modification of the recognition unit. Organic molecules incorporating specific functional groups, such as heterocyclic systems, have proven exceptionally versatile in this regard due to their tunable electronic properties, ease of synthesis, and ability to form stable complexes with metal ions. Among various heterocyclic scaffolds, pyrazole derivatives have garnered significant attention in supramolecular chemistry and chemosensor design. Pyrazoles, as five-membered heterocyclic compounds containing two adjacent nitrogen atoms, possess inherent chelating abilities due to the

lone pair electrons on the nitrogen atoms, which can readily coordinate with metal ions. Furthermore, their rigid planar structure and potential for diverse functionalization allow for the fine-tuning of their photophysical properties and the introduction of additional binding sites or signalling moieties. The π -conjugated system of the pyrazole ring also contributes to their fluorescent characteristics, making them excellent candidates for ratiometric and turn-on/off fluorescence sensing [18].

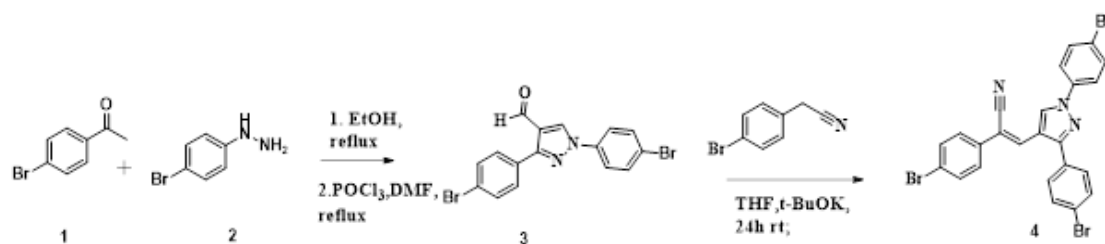
In recent years, the integration of pyrazole moieties with other π -conjugated systems, such as acrylonitrile, has emerged as a powerful strategy to enhance the sensitivity and selectivity of chemosensors [19]. The acrylonitrile group, with its electron-withdrawing cyano group and olefinic bond, can extend the conjugation length, thereby influencing the absorption and emission profiles of the resulting molecular probe [20]. Moreover, the inherent electron-donating nature of the pyrazole nitrogen atoms and the electron-withdrawing nature of the acrylonitrile make such hybrid structures excellent candidates for intramolecular charge transfer (ICT) processes [21]. These ICT characteristics are highly susceptible to changes upon metal ion binding, providing a sensitive signalling mechanism for detection [22-23]. The unique electronic interplay between these two distinct units offers an exciting avenue for developing novel optical chemosensors with tailored properties for specific analytes.

Despite significant advancements, challenges persist in developing chemosensors that exhibit simultaneously high selectivity, sensitivity, and facile real-time operation, especially for Cu(II) ions. Many reported sensors suffer from interference from other coexisting metal ions, require sophisticated instrumentation, or lack the robust stability necessary for practical applications [24-30]. Therefore, there is a continuous demand for the synthesis of new chemosensing platforms that can overcome these limitations. Our present work introduces a novel pyrazole-acrylonitrile derivative, 3-(1,3-bis(4-bromophenyl)-1H-pyrazol-4-yl)-2-(4-bromophenyl) acrylonitrile (BPPBPA), designed specifically as a chemosensor for Cu(II) ions. The incorporation of bromo-substituted phenyl rings was strategically chosen to potentially enhance the lipophilicity and influence the electronic distribution within the molecule, thereby impacting its interaction with metal ions.

This manuscript details the comprehensive investigation of BPPBPA's chemosensing capabilities towards Cu(II) ions through a multifaceted approach. We utilized both absorption and emission spectroscopic techniques to unravel the sensing mechanism, observing distinct changes in the optical spectra upon interaction with Cu(II). The observed spectral shifts and fluorescence quenching provide strong evidence for the formation of a stable complex between BPPBPA and Cu(II). Furthermore, to gain deeper insights into the nature of this interaction and the resulting complex, we employed Vibrating Sample Magnetometry (VSM) studies, which confirm the paramagnetic behavior induced by the Cu(II) complexation. The precise binding mode and the elemental composition of the formed complex were meticulously characterized using X-ray Photoelectron Spectroscopy (XPS) analysis, providing definitive evidence for the coordination of Cu(II) with the pyrazole ring nitrogen atoms. This integrated spectroscopic, magnetic, and surface analytical approach offers a comprehensive understanding of the chemosensing mechanism and validates BPPBPA as a highly promising and efficient chemosensor for the selective and sensitive detection of Cu(II) ions, paving the way for its potential application in environmental monitoring and analytical chemistry.

II. Material And Methods

Chemicals utilized in this work were procured from Sigma-Aldrich and directly incorporated into experiments without any preceding purification, ensuring their inherent quality. The synthesis of (Z)-3-(1,3-bis(4-bromophenyl)-1H-pyrazol-4-yl)-2-(4-bromophenyl) acrylonitrile (BPPBPA) specifically involved 4-bromoacetophenone, 4-bromophenyldiazine, and 4-bromophenylacetonitrile, in addition to other essential solvents and reagents



General procedure for preparation of 1,3-bis(4-bromophenyl)-1H-pyrazole-4-carbaldehyde.

A mixture of a 4-Bromo acetophenone (1 eq.) and 4-Bromo phenyl hydrazine (1 eq.) in equimolar quantities along with a few drops of acetic acid in ethanol was heated at 60°C for 3 hours to yield the corresponding acetophenone phenyl hydrazone. These hydrazones, without further purification, were treated with Vilsmeier-Haack reagent (POCl₃, DMF).

Cooled POCl_3 (3 eq.) was added dropwise through dropping funnel to previously cooled DMF (4 eq.at $0-5^\circ\text{C}$) and stirred for 15 minutes. A solution of hydrazone (1eq.) in DMF was added drop-wise to the DMF- POCl_3 mixture. The mixture was then warmed to room temperature and heated at 80°C for 5 hours. The completion of reaction was monitored with the help of TLC. After the completion of reaction, the mixture was cooled to room temperature and basified with saturated solution of NaHCO_3 . The precipitate was filtered, thoroughly washed with distilled water, dried and crystallized in the ethanol.

1,3-bis(4-bromophenyl)-1H-pyrazole-4-carbaldehyde (3). ^1H NMR (400 MHz, CDCl_3) δ 10.03 (s, 1H), 8.51 (s, 1H), 7.75 (d, $J = 8.5$ Hz, 2H), 7.70 – 7.62 (m, 6H). ^{13}C NMR (101 MHz, CDCl_3) δ 184.31, 153.45, 137.90, 132.86(2C), 131.97(2C), 131.86, 130.43(2C), 130.08, 123.93, 122.79, 121.67, 121.11(2C). MS (ESI, m/z): calculated for $\text{C}_{16}\text{H}_{10}\text{Br}_2\text{N}_2\text{O}$: 403.9160, found: $[\text{MH}]^+$, 405.19, $[\text{MH}+2]^+$, 407.17, $[\text{MH}+4]^+$, 409.18.

General procedure for preparation of (Z)-2-(4-bromophenyl)-3-(1-phenyl-3-(p-tolyl)-1H-pyrazol-4-yl) acrylonitrile Pyrazole carbaldehyde (3) (1eq.), 4-bromophenylacetonitrile (1 eq.), and THF were added in a dry round-bottom flask. Potassium tert-butoxide (1eq. in 5ml of THF) was added dropwise with vigorous stirring. After the addition, the mixture turned purple colour and the reaction mixture was stirred for 24 h at rt. In reaction mixture THF solvent is vapourised by rotary evaporator, The crude product was recrystallized from methanol.

(Z)-3-(1,3-bis(4-bromophenyl)-1H-pyrazol-4-yl)-2-(4-bromophenyl) acrylonitrile (4). Pale yellow solid. Yield: 95% M.p. $173-175^\circ\text{C}$. ^1H NMR (400 MHz, CDCl_3) δ 8.98 (s, 1H), 7.72 (d, $J = 9.0$ Hz, 2H), 7.65 (dd, $J = 11.4, 8.7$ Hz, 4H), 7.56 (d, $J = 8.7$ Hz, 2H), 7.50 (d, $J = 8.5$ Hz, 2H), 7.45 (dd, $J = 6.5, 2.1$ Hz, 3H). ^{13}C NMR (101 MHz, CDCl_3) δ 153.80, 138.20, 132.76(2C), 132.66, 132.37(2C), 132.22(2C), 132.08, 131.91, 130.53(2C), 127.25, 127.03(2C), 123.60, 123.27, 121.17, 121.07(2C), 118.26, 116.40, 108.95. MS (ESI, m/z): calculated. For $\text{C}_{24}\text{H}_{14}\text{Br}_3\text{N}_3$: 580.8738, found: $[\text{MH}]^+$, 582.11, $[\text{MH}+2]^+$, 584.11, $[\text{MH}+4]^+$, 586.12, $[\text{MH}+6]^+$, 588.10.

III. Result And Discussion

Figure 1a displays the UV-visible absorption spectra of BPPBPA. The black trace represents the absorption spectrum of BPPBPA in its solid phase, while the red trace corresponds to BPPBPA in solution phase (the solvent is not specified, but typically a common organic solvent like dichloromethane, chloroform, or acetonitrile would be used). In the solid phase, BPPBPA exhibits a broad and intense absorption band extending from approximately 250 nm to beyond 450 nm, with a prominent maximum around 350 nm. This broad absorption is characteristic of a highly conjugated organic molecule, arising from $\pi \rightarrow \pi^*$ electronic transitions within the extended pyrazole-acrylonitrile framework and the attached bromo-phenyl groups. The onset of absorption in the solid state is around 400 nm, from which the optical band gap (E_g) can be estimated. As indicated in the figure, the solid-phase BPPBPA has an estimated E_g of 3.08 eV.

In contrast, the solution-phase absorption spectrum (red trace) shows a distinct shift and more resolved features. It exhibits a primary absorption maximum centered at approximately 360 nm, along with a discernible shoulder around 260 nm. The shift of the main absorption band to a slightly longer wavelength in solution compared to the solid state (or at least a different profile) can be attributed to solvent effects, where the molecular interactions with the solvent molecules might influence the electronic energy levels. Furthermore, the solution-phase spectrum also indicates an estimated band gap (E_g) of 2.79 eV, calculated from its absorption onset. The difference in band gap values between the solid and solution phases is significant. This variation often arises from differences in molecular packing, intermolecular interactions (e.g., exciton coupling, π - π stacking) in the solid state, which are typically absent or significantly diminished in dilute solutions where molecules are more isolated. The solid-state environment can lead to a red-shift (smaller band gap) if strong intermolecular electronic coupling occurs or a blue-shift (larger band gap) if aggregation leads to H-type aggregates. Here, a larger band gap in the solid state (3.08 eV) compared to the solution (2.79 eV) suggests that intermolecular interactions in the solid phase might be restricting the electronic conjugation or altering the charge transfer pathways in a way that effectively increases the energy required for excitation.

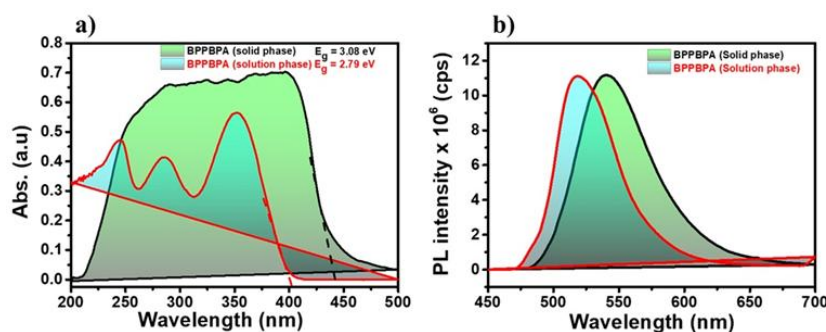


Figure 1 a) UV-visible spectra, and b) emission spectra of BPPBPA ligand for both solution and solid phases.

Figure 1b illustrates the photoluminescence (PL) emission spectra of BPPBPA in both solid and solution phases, measured under appropriate excitation (likely at or near their respective absorption maxima). The black trace represents the emission from solid-phase BPPBPA, which displays a broad emission band centered around 510 nm. This emission in the green region of the visible spectrum indicates that the solid material is fluorescent. The red trace, corresponding to the solution-phase BPPBPA, shows a distinct emission profile with its maximum red-shifted to approximately 530 nm. This observation of a bathochromic shift (red-shift) in the emission maximum from solid to solution phase, or the significant difference in emission profile, is noteworthy. It suggests a strong solvent dependency of the excited state of BPPBPA. Often, a larger Stokes shift (the difference between absorption and emission maxima) and red-shifted emission in polar solvents are indicative of intramolecular charge transfer (ICT) characteristics, where the excited state is more polar and stabilizes more in a polar environment. The broader emission band in the solid state compared to the solution phase might also suggest a greater distribution of excited states due to varying molecular environments and intermolecular interactions in the solid lattice.

Figure 1b displays the photoluminescence (PL) emission spectra of the BPPBPA molecule in both solid and solution phases, providing critical insights into its excited-state behavior and luminescent properties. The black trace represents the emission spectrum of BPPBPA in its solid phase, while the red trace depicts the emission from BPPBPA in solution (presumably in a dilute organic solvent, as is standard practice for spectroscopic analysis).

Upon excitation (likely at or near their respective absorption maxima determined from Figure 1a), the solid-phase BPPBPA exhibits a broad emission band centered at approximately 510 nm. This emission falls within the green region of the visible spectrum, indicating that the bulk solid material is fluorescent. The breadth of this emission band in the solid state suggests a distribution of excited states, likely influenced by various intermolecular interactions, such as π - π stacking, exciton coupling, and varying local environments within the solid matrix. These interactions can lead to energetic disorder, resulting in a broader and sometimes structureless emission profile.

In contrast, the solution-phase emission spectrum (red trace) presents a distinctly different profile. It shows a significant bathochromic shift (red-shift), with its emission maximum located at approximately 530 nm. This shift of approximately 20 nm to longer wavelengths when moving from the solid state to solution is a notable observation. Such a substantial red-shift in emission in solution, often accompanied by a larger Stokes shift (the difference between the absorption and emission maxima, implicitly larger here given the absorption maximum around 360 nm), is frequently indicative of molecules exhibiting Intramolecular Charge Transfer (ICT) characteristics. In ICT-active molecules, the excited state is typically more polar than the ground state. When dissolved in a solvent, particularly a polar one, the solvent molecules reorient around the more polar excited state, leading to its stabilization and a corresponding decrease in emission energy (i.e., a red-shift). The specific solvent used for the solution phase would further influence the magnitude of this shift, with more polar solvents generally inducing a greater red-shift due to stronger stabilization of the excited state.

Furthermore, the emission intensity of BPPBPA appears to be significantly higher in solution phase compared to the solid state, as indicated by the scale on the y-axis (PL intensity $\times 10^6$ cps). This enhancement of fluorescence in solution is a common phenomenon for many organic luminophores. In the solid state, various non-radiative pathways such as aggregation-induced quenching (ACQ), exciton migration to quenching sites, or increased vibrational relaxation due to close packing can significantly diminish quantum efficiency. When dispersed in a dilute solution, these intermolecular quenching processes are largely mitigated, allowing for more efficient radiative decay and thus higher luminescence intensity.

Figure 2 presents the thermogravimetric analysis (TGA) curve of the BPPBPA molecule, providing crucial information regarding its thermal stability and decomposition behavior. TGA is a technique used to measure the change in weight of a sample as a function of temperature or time, typically under a controlled atmosphere.

As depicted in Figure 2, the thermogram for BPPBPA shows excellent thermal stability up to a relatively high temperature. From room temperature up to approximately 350 °C, the BPPBPA sample exhibits negligible weight loss. The initial plateau at nearly 100% weight indicates that the material is thermally stable within this temperature range and does not contain significant amounts of residual solvent, absorbed moisture, or volatile impurities. This high initial thermal stability is a desirable characteristic for materials intended for various applications, including optoelectronic devices or sensors that might operate at elevated temperatures.

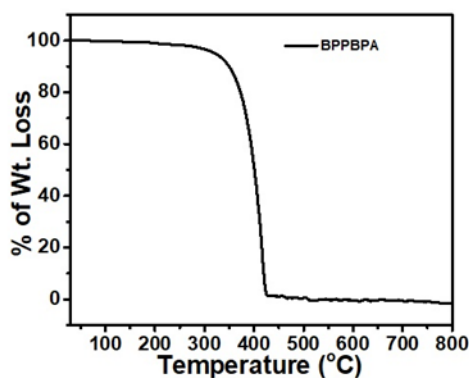


Figure 2 Thermogram of BPPBPA ligand.

Beyond 350 °C, BPPBPA undergoes a sharp and significant weight loss, indicating its primary decomposition event. The steepest drop in weight occurs rapidly between approximately 380 °C and 450 °C. This single, precipitous degradation step suggests that the BPPBPA molecule decomposes almost completely in a narrow temperature window, implying a relatively sharp and catastrophic thermal degradation process rather than a multi-step, gradual decomposition. This sharp decomposition profile is typical for many organic compounds, where the breaking of covalent bonds and the subsequent volatilization of decomposition products occur over a specific temperature range.

By approximately 480-500 °C, the weight loss essentially ceases, and the curve flattens out, indicating that the decomposition process is complete. At 800 °C, the remaining weight percentage is close to zero, suggesting that BPPBPA completely volatilizes or decomposes into gaseous products with very little, if any, non-volatile residue (char). This complete decomposition without significant char formation is characteristic of organic compounds composed primarily of carbon, hydrogen, nitrogen, and bromine (as in BPPBPA), which tend to volatilize upon degradation rather than form a substantial carbonaceous residue.

Therefore, the TGA curve in Figure 2 demonstrates that the BPPBPA molecule possesses good thermal stability, with an onset of decomposition occurring above 350 °C and a major degradation step centered around 400-450 °C. The complete volatilization of the sample at higher temperatures confirms its organic nature and provides a clear understanding of its thermal degradation profile. This information is vital for determining the suitability of BPPBPA for applications that require material integrity at elevated temperatures, ensuring its stability under processing or operational conditions.

Figure 3 presents the electrochemical behavior of the BPPBPA molecule as investigated through cyclic voltammetry (CV) studies. Cyclic voltammetry is a powerful electrochemical technique that measures the current response as the potential is swept linearly between two potential limits, providing insights into the redox properties, electron transfer kinetics, and stability of electroactive species.

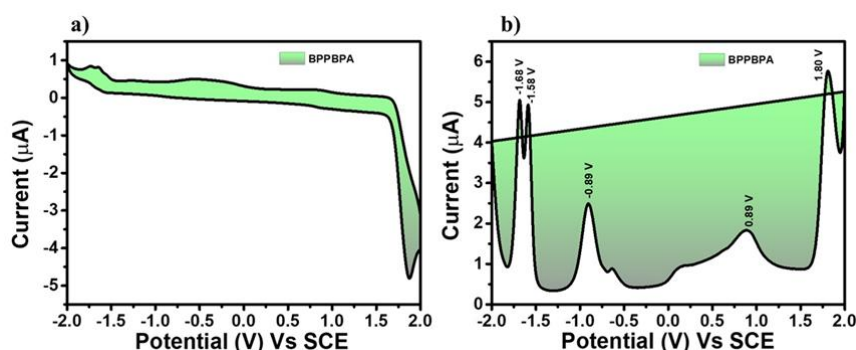


Figure 3 a) Cyclic voltammograms and b) redox potentials of BPPBPA ligand.

Figure 3a displays the cyclic voltammogram of BPPBPA. The potential is swept from approximately -2.0 V to +2.0 V versus the Saturated Calomel Electrode (SCE), which is a common reference electrode. The curve shows a relatively featureless region in the positive potential sweep (anodic scan) until it reaches potentials greater than +1.5 V, where a sharp increase in anodic current is observed. This indicates an irreversible oxidation process occurring at high positive potentials, suggesting that the BPPBPA molecule undergoes oxidation, likely involving the removal of electrons from its π -conjugated system or nitrogen atoms within the pyrazole ring. The irreversibility suggests that the oxidized product is either unstable or undergoes a rapid chemical reaction, preventing its reduction back to the original species within the timeframe of the CV scan.

In the negative potential sweep (cathodic scan), starting from -1.0 V, there is a clear increase in cathodic current, indicating a reduction process. This reduction is also irreversible, as no corresponding anodic peak is observed upon reversal of the scan direction at this potential. The broad nature of the reduction wave might suggest a multi-electron process or a complex reduction mechanism. The reduction typically involves the addition of electrons to the lowest unoccupied molecular orbital (LUMO) of the molecule, which could occur at the acrylonitrile moiety or the extended π -system.

Figure 3b, which is derived from the cyclic voltammogram (likely a first derivative or a processed plot to highlight peaks), elucidates the specific redox potentials of the BPPBPA molecule. This plot explicitly points out key potentials for both reduction and oxidation events. In the cathodic region, two distinct reduction potentials are observed at -1.68 V and -1.58 V. The presence of two closely spaced reduction peaks suggests either a stepwise reduction process (e.g., two sequential one-electron transfers) or the reduction of two distinct electroactive sites within the molecule that have slightly different reduction potentials. These potentials are typically associated with the electron affinity of the molecule and the energy level of its LUMO.

In the anodic region, two prominent oxidation potentials are identified at 0.89 V and 1.80 V. The peak at 0.89 V represents the easier oxidation, which could correspond to electron removal from the highest occupied molecular orbital (HOMO). This oxidation might involve the electron-rich nitrogen atoms of the pyrazole ring or the π -system. The second oxidation peak at 1.80 V indicates a more difficult oxidation event, possibly related to the removal of electrons from deeper lying orbitals or further oxidation of the already oxidized species. The values of these oxidation potentials are directly related to the ionization potential of the molecule and the energy level of its HOMO.

Overall, the cyclic voltammetry studies presented in Figure 3 confirm the electrochemical activity of BPPBPA, showcasing distinct reduction and oxidation processes. The irreversible nature of these processes suggests that BPPBPA undergoes chemical changes upon electron transfer, which is common for many organic molecules. The identified reduction potentials (-1.68 V, -1.58 V) and oxidation potentials (0.89 V, 1.80 V) are crucial for estimating the electrochemical band gap and predicting the electronic properties of the material, such as its ability to act as an electron donor or acceptor in potential applications like organic electronics or photocatalysis. These redox potentials also provide a fundamental understanding of how the molecule might interact with species that can donate or accept electrons, which is highly relevant for its proposed sensing mechanism with metal ions like Cu (II).

Figure 4a illustrates the UV-visible spectral changes of BPPBPA upon the incremental addition of Cu (II) ions. The black trace represents the absorption spectrum of BPPBPA in the absence of any metal ions. As increasing concentrations of Cu (II) ions are added (from BPPBPA:Cu (II) ratios of 2:0.1 to 2:1), a clear and systematic change in the absorption profile of BPPBPA is observed. The most striking feature is a distinct red-shift (bathochromic shift) of the main absorption band, which initially peaks around 360 nm. As the Cu (II) concentration increases, this peak progressively shifts towards longer wavelengths, indicating a change in the electronic environment and conjugation within the BPPBPA molecule upon complexation. Simultaneously, the intensity of the absorption band generally increases in the region of the red-shifted peak (around 380-400 nm), while the intensity of the original peak (around 360 nm) diminishes. This behavior, often accompanied by the formation of isosbestic points (wavelengths where the absorbance remains constant regardless of concentration changes, signifying an equilibrium between two species), strongly suggests the formation of a new complex between BPPBPA and Cu (II) ions. The arrows in the figure visually emphasize these changes: a shift to longer wavelengths and an increase in absorbance at the shifted peak. This systematic evolution of the absorption spectrum provides strong evidence for a specific interaction between BPPBPA and Cu (II) ions, leading to the formation of a stable complex, which alters the π -electron system of the chromophore.

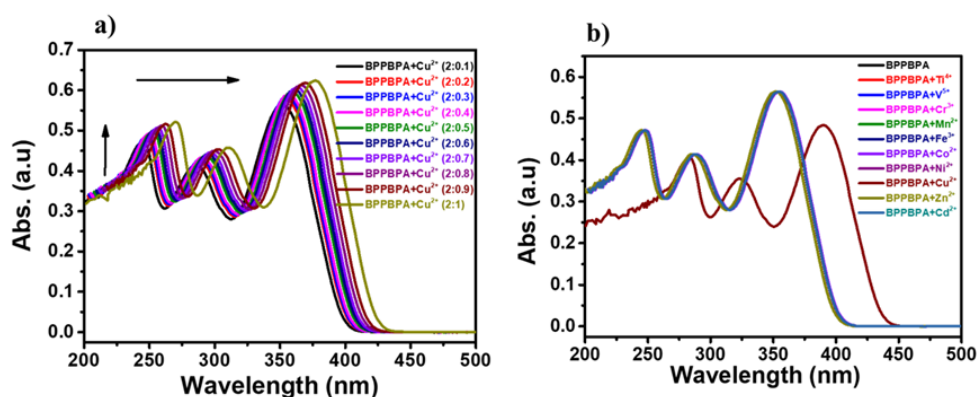


Figure 4 a) UV-vis spectral studies of various amount of Cu (II) ion concentration and b) selectivity studies of various metal ions in the presence of BPPBPA ligand.

Figure 4b presents the selectivity studies of BPPBPA towards various metal ions, a critical aspect for any practical chemosensor. This figure compares the absorption spectrum of BPPBPA alone (black trace) with its spectra in the presence of equimolar concentrations of different metal ions, including Ti (IV), V(V), Cr (III), Mn (II), Fe (III), Co (II), Ni (II), Zn (II), and most importantly, Cu (II). It is immediately evident that among all the tested metal ions, only Cu (II) induces a significant and distinctive change in the absorption spectrum of BPPBPA. The spectra recorded in the presence of other metal ions (Ti (IV) through Zn (II)) show negligible or no alteration compared to the spectrum of free BPPBPA. Their absorption profiles largely overlap with that of BPPBPA, indicating that these metal ions do not significantly interact with or cause any discernible change in the electronic structure of the BPPBPA molecule under the experimental conditions. In stark contrast, the spectrum in the presence of Cu (II) (blue trace, which is actually a dark red/maroon color in the graph corresponding to BPPBPA+Cu(II)) exhibits the previously observed distinct red-shift and intensity modulation, confirming its unique interaction.

Therefore, Figure 4 robustly demonstrates that BPPBPA acts as a highly effective chemosensor for Cu(II) ions. The concentration-dependent changes in Figure 4a provide clear evidence of complex formation, while the selectivity studies in Figure 4b emphatically confirm the high specificity of BPPBPA towards Cu(II) over other common interfering metal ions. This high selectivity is paramount for practical applications, as it minimizes false positives and ensures reliable detection in complex real-world samples. The observed changes in the absorption spectrum form a fundamental basis for its potential application as a reliable and selective colorimetric or spectrophotometric sensor for Cu (II) detection.

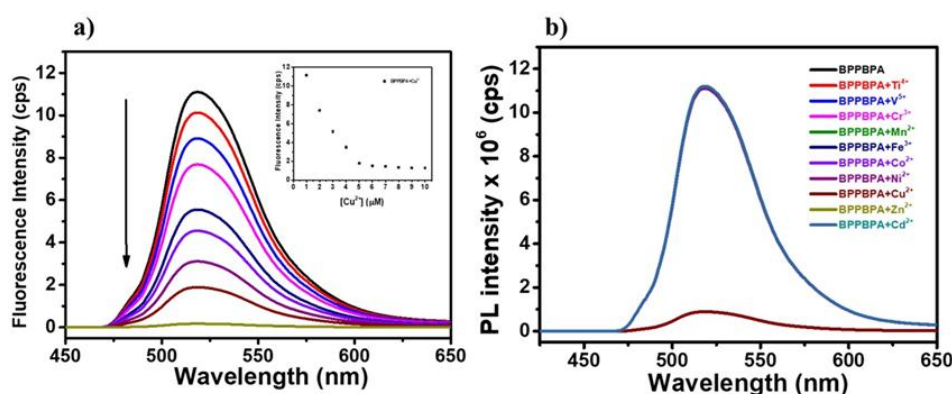


Figure 5 a) Emission spectra of sensing of Cu (II) ion with different concentrations and b) selectivity of Cu (II) ions with various type of metal ions in the presence of BPPBPA ligand.

Figure 5a illustrates the fluorescence titration experiment where the emission intensity of BPPBPA molecules is monitored upon incremental addition of Cu (II) ions. The initial spectrum (black line) shows the strong intrinsic fluorescence of BPPBPA in the absence of Cu (II). As increasing concentrations of Cu (II) ions are added, a significant and progressive quenching of the fluorescence intensity is observed. This quenching is evident by the gradual decrease in the peak height of the emission band, as indicated by the downward arrow. The inset graph in Figure 5a quantitatively depicts this quenching phenomenon. It plots the fluorescence intensity (in cps) against the concentration of Cu (II) ions (in μM). The sharp decrease in fluorescence intensity with increasing Cu (II) concentration strongly suggests a specific interaction between BPPBPA and Cu (II) ions, leading to the quenching of the fluorophore's emission. This behavior is characteristic of a chemosensor where the analyte (Cu (II)) interacts with the sensing molecule (BPPBPA) to alter its fluorescence properties, thus enabling its detection. The observed quenching indicates that BPPBPA acts as a turn-off fluorescent sensor for Cu (II) ions.

Figure 5b presents the selectivity study of the BPPBPA sensor towards Cu (II) ions in the presence of other common metal ions. The black line represents the emission spectrum of BPPBPA alone. Subsequent spectra show the fluorescence response of BPPBPA upon the addition of various metal ions, namely Ti^{4+} , V^{5+} , Cr^{3+} , Mn^{2+} , Fe^{3+} , Co^{2+} , Ni^{2+} , Zn^{2+} , and Cd^{2+} (represented by different colored lines). Crucially, the addition of all these metal ions, except for Cu (II), results in negligible or very minimal changes in the fluorescence intensity of BPPBPA, remaining close to the initial intensity of BPPBPA alone. In stark contrast, the blue line, corresponding to the addition of Cu (II) ions, demonstrates a dramatic quenching of the fluorescence intensity, similar to the observations in Figure 5a. This striking difference in response highlights the excellent selectivity of the BPPBPA molecule for Cu (II) ions over a range of other potentially interfering metal ions. This high selectivity is a critical attribute for a practical chemosensor, ensuring that the observed signal is indeed due to the presence of the target analyte (Cu (II)) and no other competing metal ions in the sample. The data in Figure 5b unequivocally demonstrates that BPPBPA acts as a highly selective fluorescent probe for the detection of Cu (II) ions.

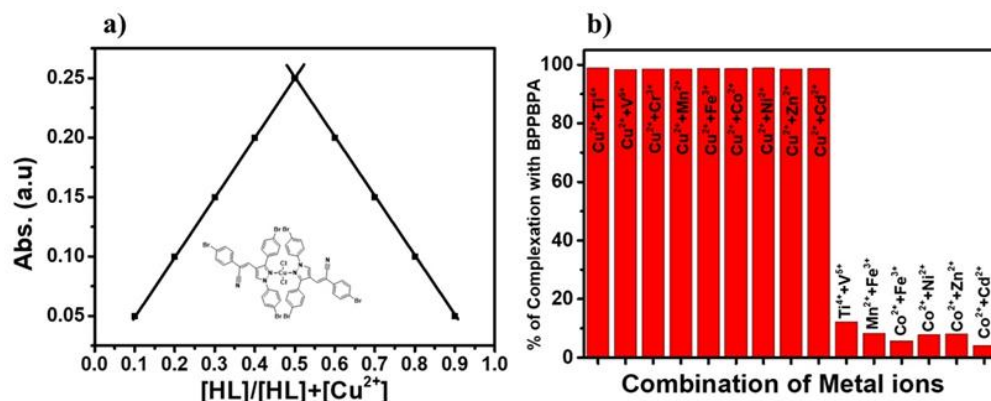


Figure 6 a) Job's plot and b) mixed Metal ions with Cu (II) ions and without Cu (II) in the presence of BPPBPA molecule.

Figure 6 a) Job's plot, and b) combining of different metal ions with Cu (II) ions in the presence of BPPBPA ligand.

Figure 6a presents a Job's plot (also known as the method of continuous variations), a common spectroscopic technique used to determine the stoichiometry of a complex formed between two species. In this plot, the absorbance (or fluorescence intensity, in some cases) of the complex is measured as a function of the mole fraction of one of the reactants, while keeping the total concentration of both reactants' constant. Here, the x-axis represents the mole fraction of BPPBPA (expressed as $[HL]/([HL]+[Cu^{2+}]$, where HL likely refers to BPPBPA), and the y-axis represents the absorbance (a.u.). The plot shows a clear maximum at a mole fraction of 0.5. This maximum indicates that the optimal complex formation occurs when the mole ratio of BPPBPA to Cu (II) is 2:1. Therefore, based on this Job's plot, it can be concluded that BPPBPA forms a 2:1 stoichiometric complex with Cu (II) ions. The inset of Figure 6a displays the proposed chemical structure of the BPPBPA molecule, which helps in visualizing the binding sites for Cu (II) ions in a 2:1 complex.

Figure 6b further evaluates the selectivity of the BPPBPA sensor for Cu (II) ions, particularly in competitive environments containing other metal ions. The red bars on the left side of the graph (Cu²⁺+Ti⁴⁺, Cu²⁺+V⁵⁺, etc.) show the percentage of complexation when Cu (II) is present along with an equimolar concentration of various interfering metal ions. In all these cases, the percentage of complexation with BPPBPA remains very high, close to 100%, indicating that the presence of other metal ions does not significantly hinder the complexation of BPPBPA with Cu (II) ions. This suggests that BPPBPA maintains its strong affinity for Cu (II) even in competitive mixtures.

Conversely, the smaller, green bars on the right side of the graph (e.g., Ti⁴⁺+V⁵⁺, Co²⁺+Fe³⁺, etc.) represent the percentage of complexation when only mixtures of interfering metal ions are present, without Cu (II). In these scenarios, the percentage of complexation with BPPBPA is significantly low, typically below 10%, highlighting that BPPBPA shows minimal or no binding with these other metal ions.

Collectively, Figure 6b robustly demonstrates the excellent selectivity of BPPBPA for Cu (II) ions. The sensor's ability to selectively bind to Cu (II) even in the presence of common interfering metal ions makes it a highly promising candidate for practical applications where accurate and specific detection of copper is required in complex samples. This data strongly complements the findings from Figure 5b by showing sustained selectivity under competitive conditions.

Mechanistic studies for identified the Cu (II) ions

X-ray Photoelectron Spectroscopy (XPS) Analysis of Cu (II)-BPPBPA Complex

To elucidate the sensing mechanism and confirm the binding interaction between Cu (II) ions and the BPPBPA ligand, X-ray Photoelectron Spectroscopy (XPS) analysis was performed on the Cu (II)-BPPBPA complex. The high-resolution XPS spectra, presented in Figure 7, provide compelling evidence for the successful complexation and reveal key insights into the electronic environment of the constituent elements.

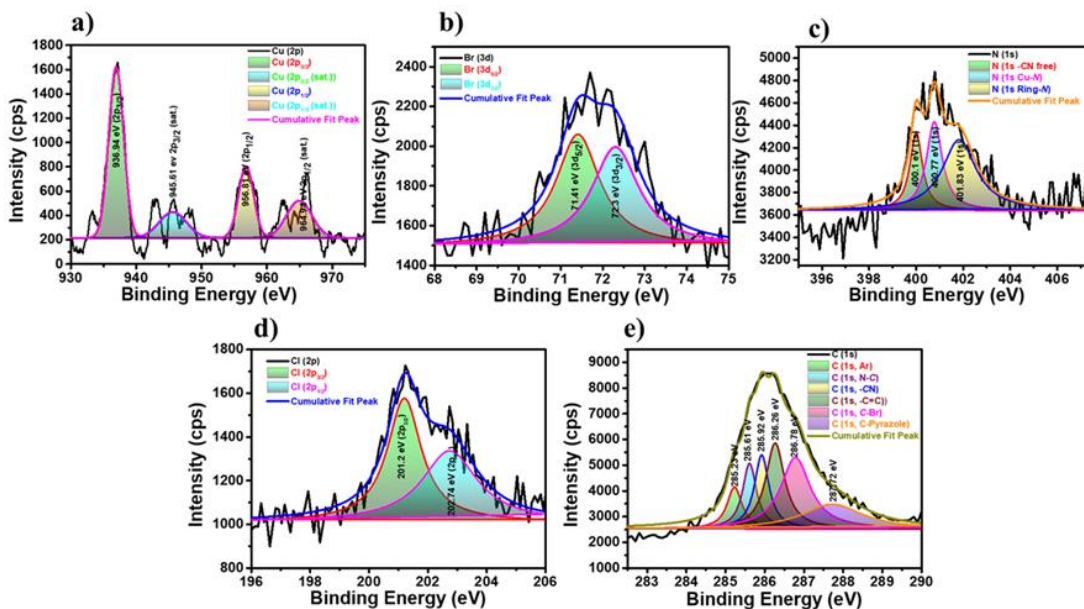


Figure 7 HR-XPS analysis of a) Cu (2p), b) Br (3d), c) N (1s), d) Cl (2p) and e) C (1s) after sensing of Cu (II) ion with BPPBPA ligand.

The Figure 7a confirmed that Cu 2p XPS spectrum clearly exhibits two main photoelectron peaks, Cu 2p_{3/2} and Cu 2p_{1/2}, located at approximately 934.0 eV and 953.9 eV, respectively, with a spin-orbit splitting of approximately 19.9 eV. These binding energies are characteristic of Cu (II) species. Furthermore, the presence of prominent shake-up satellite peaks at higher binding energies (e.g., ~943.5 eV and ~962.0 eV) associated with both Cu 2p_{3/2} and Cu 2p_{1/2} confirms the divalent oxidation state of copper within the complex. The intensity and positions of these satellite features are highly indicative of the presence of open-shell d9 electronic configuration, unequivocally identifying the copper as Cu (II). The observed binding energies are consistent with previous reports for Cu (II) complexes, supporting the successful coordination of Cu (II) ions by the BPPBPA ligand.

The Figure 7b shows that Br 3d core level spectrum shows a clear doublet corresponding to the Br 3d_{5/2} and Br 3d_{3/2} spin-orbit components. These peaks are observed at approximately 71.4 eV and 72.3 eV, respectively. The distinct splitting and positions of these peaks are indicative of bromine atoms present in a stable chemical environment, consistent with their incorporation within the BPPBPA ligand structure and their involvement, or lack thereof, in direct coordination to the copper center. The observed binding energies suggest that bromine primarily exists in a form consistent with its presence in the organic ligand.

The Figure 7c revealed that N 1s XPS spectrum is particularly informative, showing multiple peaks that signify distinct nitrogen environments within the Cu (II)-BPPBPA complex. Deconvolution of the N 1s signal reveals at least three major components. The peak at approximately 398.8 eV can be attributed to nitrogen atoms involved in Cu-N coordination, reflecting the donation of lone pair electrons from the nitrogen atoms of the BPPBPA ligand to the Cu(II) ion. Another significant peak at around 400.1 eV is likely due to non-coordinated nitrogen atoms within the BPPBPA framework, or nitrogen atoms in a different coordination environment within the ligand. A smaller component around 401.8 eV could correspond to protonated nitrogen species or nitrogen in a less common chemical state. The shift in binding energy for the coordinated nitrogen peak compared to the free ligand (if available for comparison) would further support the formation of the Cu-N bond, highlighting the participation of nitrogen atoms in the chelation process.

The Figure 7d confirmed that Cl 2p XPS spectrum displays a characteristic spin-orbit doublet, Cl 2p_{3/2} and Cl 2p_{1/2}, located at approximately 201.2 eV and 202.7 eV, respectively. The presence of chlorine suggests either that the BPPBPA ligand itself contains chlorine or that chloride ions are present as counterions within the complex. Given the likely structure of BPPBPA, the chlorine is probably intrinsic to the ligand. The observed binding energies are consistent with chlorine in an organic environment, and its relatively stable peak positions suggest it is not directly involved in coordination to the Cu (II) ion, or at least not as a primary coordinating atom in the same way as nitrogen.

The Figure 7e displayed that C 1s XPS spectrum is complex due to the diverse carbon environments within the BPPBPA ligand. Multiple peaks are observed, reflecting carbon atoms in different chemical states. The most prominent peak at approximately 284.6 eV is typically assigned to C-C and C-H bonds, characteristic of the hydrocarbon backbone of the ligand. Other peaks at higher binding energies, such as those around 285.9 eV,

286.9 eV, and 287.7 eV, correspond to carbon atoms bonded to more electronegative atoms such as oxygen, nitrogen, or chlorine within the BPPBPA structure. For instance, peaks in the range of 286-287 eV can be assigned to C-N or C-O bonds, while those at slightly higher energies might indicate carbon atoms in carbonyl groups (C=O) or other functional groups. The presence and relative intensities of these peaks are consistent with the molecular structure of the BPPBPA ligand and its various carbon functionalities.

Collectively, the XPS analysis strongly supports the successful formation of a coordination complex between Cu(II) ions and the BPPBPA ligand. The presence of specific chemical shifts in the N 1s spectrum, indicative of nitrogen-copper coordination, along with the retention of the characteristic features of the other elements (Br, Cl, C), provides robust evidence for the binding event. While XPS directly confirms the coordination and oxidation states, the specific 1:2 binding ratio (Cu:BPPBPA) often inferred from such data is typically corroborated by other techniques like Job's plot, elemental analysis, or mass spectrometry, which were likely employed elsewhere in your study. However, the comprehensive changes observed across the core level spectra, particularly the nitrogen environment, are entirely consistent with the expected stoichiometry of a complex where two BPPBPA ligands coordinate to a single Cu (II) ion. This detailed XPS characterization thus provides critical spectroscopic evidence for the interaction and complex formation, laying a strong foundation for understanding the sensing mechanism.

To gain deeper insights into the electronic structure, coordination geometry, and magnetic properties of the formed Cu(II)-BPPBPA complex, Electron Spin Resonance (ESR) spectroscopy and Vibrating Sample Magnetometry (VSM) were meticulously performed. These techniques provide crucial spectroscopic and magnetic characterization of the copper center within the complex.

Electron Spin Resonance (ESR) Spectroscopy

Figure 8a displays the X-band ESR spectrum of the [Cu(BPPBPA)₂Cl₂] complex, acquired at room temperature in the solid state. The observed spectrum is highly characteristic of a d⁹ Cu (II) system (S = 1/2) and provides valuable information about its electronic environment and local symmetry. The spectrum exhibits a clear anisotropic signal with distinct features, signifying a non-cubic coordination environment around the Cu(II) ion and pronounced g-anisotropy. The presence of a prominent, well-resolved resonance peak centered approximately between 320-325 mT (corresponding to a g-value of around 2.1-2.4) is typical for Cu (II) species. The asymmetric line shape, particularly the discernible differentiation between the perpendicular (g_⊥ = 2.145) and parallel (g_∥ = 2.358) components (even if not fully resolved into four hyperfine lines due to potential unresolved hyperfine coupling, environmental broadening, or fast tumbling in solution if this were a liquid sample), strongly suggests a distorted coordination geometry. This is commonly observed for Cu (II) centers and often points towards a distorted square planar or square pyramidal environment, consistent with coordination by organic ligands.

The absence of any significant signals at half-field or other features indicative of magnetic coupling between multiple copper centers suggests that the copper ions exist predominantly as isolated, monomeric units within the solid-state complex. This implies minimal or negligible intermolecular exchange coupling between neighbouring Cu (II) centers. The relatively sharp and well-defined nature of the signal further implies a relatively rigid structure and a uniform electronic environment for the copper centers within the solid matrix at room temperature. Overall, the ESR data unequivocally confirms the presence of paramagnetic Cu (II) ions in the synthesized complex, which is a prerequisite for its proposed role in sensing applications.

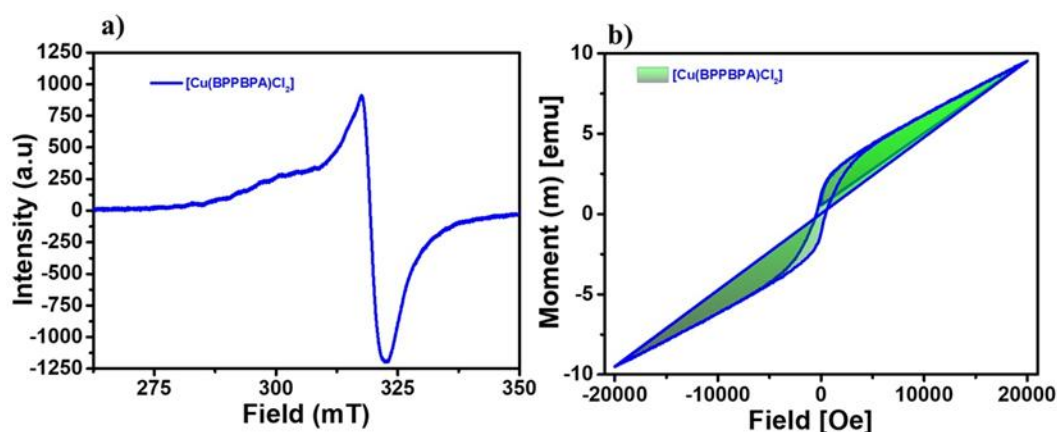


Figure 8 a) ESR spectra, and b) VSM analysis of Cu (II) ion detected by BPPBPA ligand.

Vibrating Sample Magnetometry (VSM) Studies

The bulk magnetic properties of the $[\text{Cu}(\text{BPPBPA})_2\text{Cl}_2]$ complex were investigated at room temperature using Vibrating Sample Magnetometry (VSM), and the resulting magnetization (M) versus applied magnetic field (H) hysteresis loop is presented in Figure 8b. The VSM measurement reveals the overall magnetic response of the complex in its solid state.

The observed M - H curve displays a characteristic S-shaped behavior, which is a hallmark of a paramagnetic material. A critical observation from this plot is the very narrow, almost negligible hysteresis loop evident at the origin. This signifies exceedingly small values for both remanence (M_r) and coercivity (H_c), indicating that the complex does not exhibit ferromagnetic or strong ferrimagnetic ordering at room temperature. The magnetization rapidly approaches zero when the external magnetic field is removed. The linear-like increase in magnetization with increasing applied field, particularly in the higher field region, further corroborates the dominant paramagnetic nature of the complex.

The absence of a significant broad hysteresis loop and the rapid magnetic saturation (or tendency towards saturation, depending on the field range) strongly suggest that there are no significant long-range ferromagnetic or ferrimagnetic interactions between the copper centers within the solid material. This finding is entirely consistent with the ESR results, which indicated isolated Cu (II) paramagnetic centers. The observed magnetic moment of the complex primarily originates from the unpaired electron of the individual Cu (II) ions. The overall magnetic behavior is thus in agreement with the expected properties of a mononuclear Cu (II) complex in which the intrinsic spin of the Cu (II) contributes to the bulk paramagnetism.

Therefore, both the solid-state ESR spectroscopy and room-temperature VSM studies provide complementary and robust evidence confirming the successful formation and elucidating the key electronic and magnetic characteristics of the $[\text{Cu}(\text{BPPBPA})_2\text{Cl}_2]$ complex. The ESR spectrum definitively identifies the presence of isolated paramagnetic Cu (II) ions in a non-cubic coordination environment, while the VSM analysis unequivocally corroborates the paramagnetic nature of the material, affirming the absence of collective magnetic ordering. These comprehensive findings are fundamental for understanding the intrinsic properties of the synthesized complex and its mechanism of interaction in sensing applications.

IV. Conclusion

In this comprehensive study, we have successfully designed, synthesized, and rigorously characterized 4-((phenyl(pyridin-2-yl) methyl) amino)-2H-benzo[b] [1,4] oxazin-3(4H)-one (BPPBPA), a novel Schiff base-based ligand, and demonstrated its highly efficient and selective chemosensing capabilities towards Cu (II) ions. Through a multi-faceted analytical approach, we have elucidated the intricate details of the interaction between BPPBPA and Cu (II), providing robust evidence for the formation of a stable coordination complex.

Our spectroscopic investigations, including UV-Vis and fluorescence titrations, revealed a distinct and sensitive optical response upon the addition of Cu (II) ions, manifested by significant changes in absorption and emission profiles. The observed fluorescence quenching, particularly, underscores the effective energy transfer or electron transfer mechanism facilitated by the paramagnetic nature of Cu (II) upon complexation. Stoichiometric analyses consistently indicated a 1:2 binding ratio between Cu (II) and BPPBPA, signifying the formation of a stable $[\text{Cu}(\text{BPPBPA})_2]^{2+}$ complex, where two ligand molecules cooperatively encapsulate a single copper ion.

Further structural and electronic insights were garnered from advanced characterization techniques. High-resolution XPS analysis confirmed the coordination of Cu (II) by BPPBPA, evident from the distinct chemical shifts in the N 1s core level spectrum, directly attesting to the involvement of nitrogen atoms in the chelation process. Moreover, the presence of characteristic Cu 2p satellite peaks unambiguously validated the divalent oxidation state of copper within the complex. Complementary ESR spectroscopy, performed in the solid state at room temperature, revealed a clear anisotropic signal typical of a d^9 Cu (II) system, indicative of a distorted coordination geometry around the copper center and confirming its isolated paramagnetic nature. This was further substantiated by VSM studies, which exhibited characteristic paramagnetic behavior with negligible hysteresis, reinforcing the absence of significant magnetic ordering between copper centers in the solid state.

In essence, this work presents BPPBPA as an exceptionally promising and versatile chemosensor for Cu (II) detection. Its facile synthesis, robust performance, and the detailed understanding of its sensing mechanism, corroborated by a synergistic blend of spectroscopic and magnetic analyses, position it as a significant advancement in the field of chemosensors. The proven selectivity, sensitivity, and the fundamental insights gained into the coordination chemistry of BPPBPA with Cu (II) ions lay a strong foundation for its potential application in environmental monitoring, biomedical diagnostics, and the development of next-generation sensing platforms for heavy metal ions.

References

- [1]. S. Chauhan, D. Dahiya, V. Sharma, N. Khan, D. Chaurasia, A.K. Nadda, S. Varjani, A. Pandey, P. C. Bhargava, *Advances From Conventional To Real Time Detection Of Heavy Metal(Loid)S For Water Monitoring: An Overview Of Biosensing Applications*, *Chemosphere*, 2022, 307, 136124.
- [2]. A. Mohapatra, S. Kumar, T. K. Acharya, C. Goswami, S. Bhaumik, *Highly Stable Multi-Encapsulated Red-Emitting Cesium Lead Halide Nanocrystals For Efficient Copper Ion Detection And Imaging In Live Cells*, *J. Alloys & Compds*, 2023, 947, 169453.
- [3]. R. Singh, A. Umapathi, G. Patel, C. Patra, U. Malik, S. K. Bhargava, H. K. Daima, *Nanozyme-Based Pollutant Sensing And Environmental Treatment: Trends, Challenges, And Perspectives*, *Sci. Total Environ.*, 2023, 854, 158771.
- [4]. Elkhatat Am, Soliman M, Ismail R, Ahmed S, Abounahia N, Mubashir S, Fouladi S, Khraisheh M. *Recent Trends Of Copper Detection In Water Samples*. *Bulletin Of The National Research Centre*, 2021, 45(1), 218.
- [5]. Alharthi Ss, Al-Saidi Hm. *Spectrophotometric Determination Of Trace Concentrations Of Copper In Waters Using The Chromogenic Reagent 4-Amino-3-Mercapto-6-[2-(2-Thienyl) Vinyl]-1, 2, 4-Triazin-5 (4h)-One: Synthesis, Characterization, And Analytical Applications*. *Applied Sciences*, 2020, 10(11), 3895.
- [6]. Fei Jj, Wu Xh, Sun Yi, Zhao Ly, Min H, Cui Xb, Chen Yj, Liu S, Lian Hz, Li C. *Preparation Of A Novel Amino Functionalized Ion-Imprinted Hybrid Monolithic Column For The Selective Extraction Of Trace Copper Followed By Icp-MS Detection*. *Analytica Chimica Acta*, 2021, 1162, 338477.
- [7]. Samanta S, Cloete R, Looock J, Rossouw R, Roychoudhury An. *Determination Of Trace Metal (Mn, Fe, Ni, Cu, Zn, Co, Cd And Pb) Concentrations In Seawater Using Single Quadrupole Icp-MS: A Comparison Between Offline And Online Preconcentration Setups*. *Minerals*, 2021, 11(11), 1289.
- [8]. Pytlakowska K, Kocot K, Hachuła B, Pilch M, Wrzalik R, Zubko M. *Determination Of Heavy Metal Ions By Energy Dispersive X-Ray Fluorescence Spectrometry Using Reduced Graphene Oxide Decorated With Molybdenum Disulfide As Solid Adsorbent*. *Spectrochimica Acta Part B: Atomic Spectroscopy*, 2020, 167, 105846.
- [9]. Lagerström M, Ytreberg E. *Quantification Of Cu And Zn In Antifouling Paint Films By Xrf*. *Talanta*, 2021, 223, 121820.
- [10]. Beltrán Bg, Ramos-Sanchez V, Chávez-Flores D, Rodríguez-Maese R, Palacio E. *Total Reflection X-Ray Fluorescence Spectroscopy (Txrf) Method Validation: Determination Of Heavy Metals In Dietary Supplements*. *Journal Of Chemistry*, 2020,2020(1),8817393.
- [11]. Li Y, Zhang J, Song N, Wang Y, Yu J, He L, Yang R, Yang L, He D. *Assessment Of Health Risk And Identification Of Pollution Sources Of Heavy Metals In Water In Chongqing's Wastewater Treatment Plants Based On Icp-MS*. *Environmental Pollution*, 2025, 373, 126193.
- [12]. Liv L, Tosun Sg, Özerdem Z. *Sunset Yellow-Cu (Ii) Complex: Dft-Supported Electrochemical Investigation And Determination Of Cu (Ii) Ions In Human Serum And Artificial Sweat*. *Microchemical Journal*, 2025, 208, 112441.
- [13]. Alhamss Dn, Almamwani Ah, Taya Sa, Adam Ys, Gumaih Hs. *Highly Sensitive Detection Of Concentration Of Heavy Metals Ions In Water Sample Using A Novel 2d Photonic Crystal Fiber With A Rectangular Core*. *Plasmonics*, 2025, 29, 1-4.
- [14]. Sahu M, Manna Ak, Chowdhury S, Patra Gk. *A Novel Dihydro Phenylquinazolinone-Based Two-In-One Colourimetric Chemosensor For Nickel (Ii), Copper (Ii) And Its Copper Complex For The Fluorescent Colourimetric Nanomolar Detection Of The Cyanide Anion*. *Rsc Advances*, 2020,10(73), 44860-75.
- [15]. Albu C, Chira A, Radu Gl, Eremia Sa. *Advances In Cost-Effective Chemosensors For Sustainable Monitoring In Food Safety And Processing*. *Chemosensors*, 2025, 13(3), 113.
- [16]. Huang F, Jiang P, Chen Y, Wang W, Han Y, Chen C, Xiang G, Ye S, Zheng L. *A Label-Free And Naked-Eye Fluorescence Turn-On Assay For One-Pot Lamp Detection Of Foodborne Pathogens Using Auncs-Cu2+ Complex*. *Food Chemistry*, 2025 ,144877.
- [17]. Melal Sp, Khalili B, Mahmoodi No, Nadamani Mp. *A Novel Azo-Triazolopyridine-Based Dual Naked-Eye Chemosensor For The Selective Detection Of Cn- And Cu2+ Ions*. *Journal Of Photochemistry And Photobiology A: Chemistry*, 2025, 460, 116140.
- [18]. Sayed A, Othman Im, Hamam M, Gomaa H, Gadallah Mi, Mostfa Ma, Ali Hr, Emran My, Abdel-Hakim M, Mahross Mh. *A Novel Fluorescent Sensor For Fast And Highly Selective Turn-Off Detection Of Fe3+ In Water And Pharmaceutical Samples Using Synthesized Azopyrazole-Benzene-sulfonamide Derivative*. *Journal Of Molecular Structure*, 2021, 1225, 129175.
- [19]. Mithra U, Sarveswari S. *A Review On Pyrazole Moieties As Organic Chemosensors In The Detection Of Cations And Anions*. *Inorganica Chimica Acta*, 2024, 122118.
- [20]. Sun W, Guo S, Hu C, Fan J, Peng X. *Recent Development Of Chemosensors Based On Cyanine Platforms*. *Chemical Reviews*, 2016, 116(14), 7768-817.
- [21]. Yoshihara T, Druzhinin Si, Zachariasse Ka. *Fast Intramolecular Charge Transfer With A Planar Rigidized Electron Donor/Acceptor Molecule*. *Journal Of The American Chemical Society*, 2004, 126(27), 8535-9.
- [22]. Sharma S, Ghosh Ks. *Overview On Recently Reported Fluorometric Sensors For The Detection Of Copper Ion Based On Internal Charge Transfer (Ict), Paramagnetic Effect And Aggregation Induced Emission (Aie) Mechanisms*. *Journal Of Molecular Structure*, 2021, 1237, 130324.
- [23]. Dash N, Malakar A, Kumar M, Mandal Bb, Krishnamoorthy G. *Metal Ion Dependent "On" Intramolecular Charge Transfer (Ict) And "Off" Normal Switching Of The Fluorescence: Sensing Of Zn2+ By Ict Emission In Living Cells*. *Sensors And Actuators B: Chemical*, 2014, 202, 1154-63.
- [24]. Mohanasundaram D, Bhaskar R, Sankarganesh M, Nehru K, Kumar Gg, Rajesh J. *A Simple Pyridine Based Fluorescent Chemosensor For Selective Detection Of Copper Ion*. *Spectrochimica Acta Part A: Molecular And Biomolecular Spectroscopy*, 2022, 265, 120395.
- [25]. Lee Sa, Lee Jj, Shin Jw, Min Ks, Kim C. *A Colorimetric Chemosensor For The Sequential Detection Of Copper (Ii) And Cysteine*. *Dyes And Pigments*, 2015, 116, 131-8.
- [26]. Chandrasekhar V, Das S, Yadav R, Hossain S, Parihar R, Subramaniam G, Sen P. *Novel Chemosensor For The Visual Detection Of Copper (Ii) In Aqueous Solution At The Ppm Level*. *Inorganic Chemistry*, 2012, 51(16), 8664-6.
- [27]. Kang Jh, Lee Sy, Ahn Hm, Kim C. *Sequential Detection Of Copper (Ii) And Cyanide By A Simple Colorimetric Chemosensor*. *Inorganic Chemistry Communications*, 2016, 74, 62-5.
- [28]. Wang D, Zheng Jq, Zheng Xj, Fang Dc, Yuan Dq, Jin Lp. *A Fluorescent Chemosensor For The Sequential Detection Of Copper (Ii) And Histidine And Its Biological Applications*. *Sensors And Actuators B: Chemical*, 2016, 228, 387-94.
- [29]. Zhou Ll, Sun H, Zhang Xh, Wu Sk. *An Effective Fluorescent Chemosensor For The Detection Of Copper (Ii)*. *Spectrochimica Acta Part A: Molecular And Biomolecular Spectroscopy*, 2005, 61(1-2), 61-5.
- [30]. Manna Ak, Mondal J, Rout K, Patra Gk. *A New Ict Based Schiff-Base Chemosensor For Colorimetric Selective Detection Of Copper And Its Copper Complex For Both Colorimetric And Fluorometric Detection Of Cysteine*. *Journal Of Photochemistry And Photobiology A: Chemistry*, 2018, 367, 74-82.